Meson phenomenology and phase transitions in nonlocal chiral quark models

2015 J. Phys.: Conf. Ser. 630 012049

(http://iopscience.iop.org/1742-6596/630/1/012049)

Journal of Physics: Conference Series **630** (2015) 012049 doi:10.1088/1742-6596/630/1/012049

Meson phenomenology and phase transitions in nonlocal chiral quark models

J P Carlomagno[a,b], D Gómez Dumm[a,b], V Pagura[a,b] and N N Scoccola[b,c,d]

[a] IFLP, CONICET − Dpto. de Física, FCE, Universidad Nacional de La Plata, C.C. 67, 1900 La Plata, Argentina
[b] CONICET, Rivadavia 1917, 1033 Buenos Aires, Argentina
[c] Physics Department, Comisión Nacional de Energía Atmica, Av.Libertador 8250, 1429 Buenos Aires, Argentina
[d] Universidad Favaloro, Solís 453, 1078 Buenos Aires, Argentina

E-mail: dumm@fisica.unlp.edu.ar

Abstract. We study the features of nonlocal chiral quark models that include wave function renormalization. Model parameters are determined from meson phenomenology, considering different nonlocal form factor shapes. In this context we analyze the characteristics of the deconfinement and chiral restoration transitions at finite temperature and chemical potential, introducing the couplings of fermions to the Polyakov loop for different Polyakov potentials. The results for various thermodynamical quantities are compared with data obtained from lattice QCD calculations.

1. Introduction

The detailed understanding of the behavior of strongly interacting matter under extreme conditions of temperature and/or density has become an issue of great interest in recent years. It is widely believed that as the temperature and/or density increase, one finds a transition from a hadronic phase to a partonic one, in which chiral symmetry is restored. From the theoretical point of view, one way to address the study of these phase transitions is through lattice QCD calculations [1, 2, 3]. However, this ab-initio approach shows difficulties when dealing with small current quark masses and finite real chemical potentials. Thus it is worth to develop effective models that show consistency with lattice results, and can be extrapolated into regions not accessible by lattice calculation techniques. Here we will concentrate on one particular class of effective theories, namely the so-called nonlocal Polyakov−Nambu−Jona-Lasinio (nlPNJL) models [4, 5, 6, 7, 8], in which quarks move in a background color field and interact through covariant nonlocal chirally symmetric four-point couplings.

The aim of this work is to study the chiral restoration and deconfinement transitions at nonzero temperature and both real and imaginary chemical potentials, taking into account the effect of dynamical quarks on the Polyakov loop (PL) effective potential [9, 10, 11]. We consider both SU(2) chiral models and the corresponding extension to three flavors, including flavor mixing through a nonlocal 't Hooft-like six-fermion interaction [12, 13, 14]. Special attention is paid to models in which the nonlocal form factors are chosen on the basis of lattice QCD results

for the effective quark propagators. This requires the inclusion of a nonlocal interaction that leads to wave function renormalization (WFR) of the quark fields [15].

2. Meson phenomenology

We start by considering a chiral quark model in which the Lagrangian includes the coupling between quark-antiquark nonlocal currents. The explicit expression for this Lagrangian for the three-flavor case (including WFR) can be found in Ref. [14]. Now, in order to work with mesonic degrees of freedom, we proceed to perform a standard bosonization of the fermionic theory, introducing scalar and pseudoscalar fields. After integrating out the fermionic degrees of freedom, we expand the bosonic fields around their vacuum expectation values. At this mean field level the Euclidean effective action reduces to

$$\frac{S_E^{\rm MFA}}{V^{(4)}} = -2\ {\rm Tr}\ \int \frac{d^4p}{(2\pi)^4} \log\left[\frac{M(p)^2+p^2}{Z(p)^2}\right] - \bar{\sigma}_a \bar{S}_a - \bar{\zeta}\bar{R} - \frac{G}{2}(\bar{S}_a\bar{S}_a + \bar{R}^2) - \frac{H}{4} A_{abc}\bar{S}_a\bar{S}_b\bar{S}_c\ , \quad (1)$$

where G and H are the coupling constants corresponding to the four- and six-fermion nonlocal interactions, respectively, and the trace acts over color and flavor spaces. The mean field values of the scalar fields $\bar{\sigma}_a$ and $\bar{\zeta}$, and the auxiliary fields $\bar{S}_a$, $\bar{P}_a$ and $\bar{R}$ are obtained through the minimization of the partition function and the usage of the random phase approximation, in the path integral formalism. This leads to a set of coupled gap equations that can be found in Ref. [14]. The functions $M_i(p)$ and $Z(p)$ correspond to momentum-dependent effective masses and WFR of the quark propagators. In terms of the model parameters and form factors, these are given by

$$M_i(p) = Z(p)\ [m_i\ +\ \bar{\sigma}_i\, g(p)]\ , \quad Z(p) = \left[1\ -\ \kappa^{-1}\bar{\zeta}\, f(p)\right]^{-1}\ , \quad i = u,d,s\ , \quad (2)$$

where κ is a parameter that controls the relative weight of the coupling leading to the WFR, m_i are the current quark masses, and $f(p)$ and $g(p)$ are the fourier transforms of the nonlocal form factors in the quark-antiquark currents.

In order to analyze the properties of meson fields it is necessary to go beyond the mean field level, considering quadratic fluctuations in the Euclidean action:

$$S_E^{\rm quad} \ = \ \frac{1}{2}\int \frac{d^4p}{(2\pi)^4} \sum_M\ r_M\ G_M(p^2)\ \phi_M(p)\,\bar{\phi}_M(-p)\ , \quad (3)$$

where ϕ_M stand for the meson fields in the charge basis, M being the scalar and pseudoscalar mesons in the lowest mass nonets, plus the ζ field. The coefficient r_M is 1 for charge eigenstates $M = {\rm a}_0^0, \sigma, f_0, \zeta, \pi^0, \eta, \eta'$, and 2 for $M = {\rm a}_0^+, \kappa, K_0^*, \pi^+, K^+, K^0$. Thus meson masses are given by the equations

$$G_M(-m_M^2)\ =\ 0\ . \quad (4)$$

Full expressions for the one-loop functions $G_M(q)$ can be found in Refs. [13, 14].

The model includes five parameters, namely the current quark masses $m_{u,s}$ and the coupling constants G, H and κ. In addition, one has to specify the form factors $g(p)$ and $f(p)$. We will consider here two parametrizations, corresponding to different functional forms for the form factors: the first one (PI) involves the often used exponential functions,

$$g(p) = \exp\left(-p^2/\Lambda_0^2\right)\ , \qquad f(p) = \exp\left(-p^2/\Lambda_1^2\right)\ , \quad (5)$$

while for the second one (PII) we use the functions [15]

$$g(p) = \frac{1+\alpha_z}{1+\alpha_z\ f_z(p)}\,\frac{\alpha_m\ f_m(p) - m_u\ \alpha_z f_z(p)}{\alpha_m - m_u\ \alpha_z}\ , \qquad f(p) = \frac{1+\alpha_z}{1+\alpha_z\ f_z(p)} f_z(p)\ , \quad (6)$$

where

$$f_m(p) = \left[1 + \left(p^2/\Lambda_0^2\right)^{3/2}\right]^{-1} , \qquad f_z(p) = \left[1 + \left(p^2/\Lambda_1^2\right)\right]^{-5/2} , \tag{7}$$

with $\bar{\sigma}_u = (\alpha_m - m_u\alpha_z)/(1+\alpha_z)$, $\bar{\zeta} = \kappa\alpha_z/(1+\alpha_z)$.

Given the form factor functions, one can fix the model parameters (see Ref. [14]) so as to reproduce the observed meson phenomenology. To the above mentioned parameters $m_{u,s}$, G, H and κ one has to add the cutoff scales Λ_0 and Λ_1, introduced through the form factors. We have taken as input some selected observables, such as the pion and kaon masses. As it is shown in Fig. 1, the functions defined by the parametrization PII allow to fit adequately the momentum dependence of mass and WFR in the light quark propagators to the results obtained in lattice QCD calculations [16].

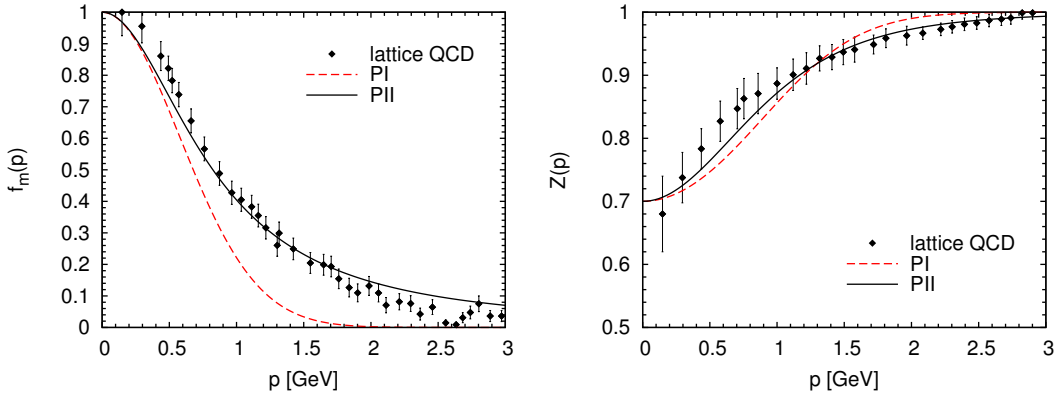

Figure 1. Momentum dependences for mass and WFR for our parameterizations PI and PII, in comparison with lattice results from Ref. [16].

Once the parameters have been determined, we can calculate the values of several meson properties for the scalar and pseudoscalar sector. The parameter values for PI and PII are given in Table 1 and our numerical results are quoted in Table 2, where input observables are indicated. In general, it is seen that the meson masses, mixing angles and weak decay constants predicted by the model are in a reasonable agreement with phenomenological expectations. Moreover, the results for PI do not differ significantly from those obtained in Ref. [6] for a nlPNJL model with a Gaussian form factor $g(p)$ and no WFR (we call this parametrization PIII).

	PI	PII
m_u [MeV]	5.7	2.6
m_s [MeV]	136	65
Λ_0	814	799
Λ_1 [MeV]	1033	1570
$G\,\Lambda_0^2$	23.6	16.6
$H\,\Lambda_0^5$	-526	-202
κ/Λ_0	5.36	11.1

Table 1. Parameter values for PI and PII.

$\bar{\sigma}_u$ [MeV]	529	469	-
$\bar{\sigma}_s$ [MeV]	702	707	-
$\bar{\zeta}/\kappa$	-0.429	-0.429	-
$-\langle\bar{u}u\rangle^{1/3}$ [MeV]	240	316	-
$-\langle\bar{s}s\rangle^{1/3}$ [MeV]	198	340	-
m_π [MeV]	input	input	139
m_K [MeV]	input	input	495
m_η [MeV]	527	522	547
$m_{\eta'}$ [MeV]	input	input	958
m_σ	601	561	$400-550$
m_κ [MeV]	810	732	$650-710$
f_π [MeV]	input	input	92.4
f_K/f_π	1.17	1.17	1.22
f_η^0/f_π	0.17	0.21	(0.11 - 0.507)
f_η^8/f_π	1.12	1.08	(1.17 - 1.22)
$f_{\eta'}^0/f_\pi$	1.09	1.54	(0.98 - 1.16)
$f_{\eta'}^8/f_\pi$	-0.48	-0.48	$-$(0.42 - 0.46)
θ_0	-8.63°	-7.91°	$-(0^\circ$ - $10^\circ)$
θ_8	-22.9°	-23.7°	$-(19^\circ$ - $22^\circ)$

Table 2. Results for various phenomenological quantities within nonlocal models for parametrizations PI and PII.

3. Nonzero temperature

In order to investigate the phase transitions and the temperature dependence of thermodynamical quantities within our model, we consider the thermodynamical potential per unit volume at the mean field level. In order to deal with the interaction between quarks and color gauge fields we assume that quarks move on a constant background field $\phi = A_4 = iA_0 = ig\,\delta_{\mu 0}\,G_a^\mu\lambda^a/2$, where G_a^μ are the SU(3) color gauge fields and λ_a are the Gell-Mann matrices. Then the traced Polyakov loop, which in the infinite quark mass limit can be taken as order parameter of confinement, is given by $\Phi = \frac{1}{3}\mathrm{Tr}\,\exp(i\phi/T)$.

We proceed by using the standard Matsubara formalism. The mean field thermodynamical potential will be given by

$$\Omega^{\rm MFA} \;=\; \Omega^{\rm reg} + \Omega^{\rm free} + \mathcal{U}(\Phi,T)\;, \tag{8}$$

where

$$\begin{aligned}
\Omega^{\rm reg} &= -2\,T\sum_{n=-\infty}^{\infty}\sum_{c,f}\int\frac{d^3p}{(2\pi)^3}\;\log\left[\frac{p_{nc}^2+M_f^2(p_{nc})}{Z^2(p_{nc})\,(p_{nc}^2+m_f^2)}\right] \\
&\quad -\left(\bar{\zeta}\,\bar{R}+\frac{G}{2}\,\bar{R}^2+\frac{H}{4}\,\bar{S}_u\,\bar{S}_d\,\bar{S}_s\right)-\frac{1}{2}\sum_f\left(\bar{\sigma}_f\bar{S}_f+\frac{G}{2}\,\bar{S}_f^2\right)\;, \\
\Omega^{\rm free} &= -2\,T\sum_{c,f}\sum_{s=\pm1}\int\frac{d^3p}{(2\pi)^3}\;\mathrm{Re}\,\log\left[1+\exp\left(-\frac{\epsilon_{fp}+\imath\,s\,\phi_c}{T}\right)\right]\;.
\end{aligned} \tag{9}$$

Here we have defined $p_{nc}^2 = [(2n+1)\pi T+\phi_c]^2+\vec{p}^{\,2}$, $\epsilon_{fp} = \sqrt{\vec{p}^{\,2}+m_f^2}$. The sums over color and flavor indices run over $c = r,g,b$ and $f = u,d,s$, respectively, and the color background fields are $\phi_r = -\phi_g = \phi_3$, $\phi_b = 0$. The term $\mathcal{U}(\Phi,T)$ is known as the Polyakov-loop potential, which accounts for effective gauge field self-interactions. It is usual to take for this potential a functional form based on properties of pure gauge QCD. One possible ansatz is that based on the

logarithmic expression of the Haar measure associated with the SU(3) color group integration. This yields [17]

$$\frac{\mathcal{U}_{\log}(\Phi,T)}{T^4} \;=\; -\frac{1}{2}\,a(T)\,\Phi^2 \;+\; b(T)\,\log\left(1-6\,\Phi^2+8\,\Phi^3-3\,\Phi^4\right)\;, \tag{10}$$

where

$$a(T) = a_0 + a_1\left(\frac{T_0}{T}\right) + a_2\left(\frac{T_0}{T}\right)^2\;, \qquad b(T) = b_3\left(\frac{T_0}{T}\right)^3\;. \tag{11}$$

The parameters in the above expression can be fitted to pure gauge lattice QCD data so as to properly reproduce the corresponding equation of state and Polyakov loop behavior [17]. In absence of dynamical quarks T_0 is the deconfinement temperature, which is expected to be about 270 MeV from lattice calculations. However, it has been argued that in the presence of light dynamical quarks this temperature scale should be adequately reduced to about 210 and 190 MeV for the case of two and three flavors, respectively, with an uncertainty of about 30 MeV [18]. Besides the logarithmic function in Eq. (10), other possible forms for the Polyakov-loop potential can be found in Ref. [14].

In order to analyze the phase transitions it is useful to define a subtracted quark condensate

$$\langle\bar{q}q\rangle_{\rm sub} \;=\; \frac{\langle\bar{u}u\rangle \;-\; \frac{m_u}{m_s}\,\langle\bar{s}s\rangle}{\langle\bar{u}u\rangle_0 \;-\; \frac{m_u}{m_s}\,\langle\bar{s}s\rangle_0}\;, \tag{12}$$

where $\langle\bar{q}q\rangle_0$ are the values of the chiral condensates at zero temperature. In Fig. 2 we quote our results for the subtracted quark condensate and the Polyakov loop, together with the corresponding susceptibilities, as functions of the temperature. The values correspond to PII and the PL potential given by Eq. (10), taking $T_0 = 270$ and 200 MeV. For comparison we include lattice QCD results from Refs. [19, 20]. As expected, it is found that when the temperature is increased the system undergoes both a chiral restoration and deconfinement transitions, which proceed as smooth crossovers. It is seen that both transitions occur essentially at the same critical temperatures, in agreement with lattice QCD results. The numerical values are $T_c \simeq 200$ MeV and $T_c \simeq 165$ MeV for $T_0 = 270$ and 200 MeV, respectively, while lattice QCD analyses lead to a transition temperature of about 160 MeV [19, 20]. Thus, the agreement with lattice QCD data favors the suggested rescaling of the reference temperature T_0 from the pure gauge transition temperature (270 MeV) towards values around 200 MeV.

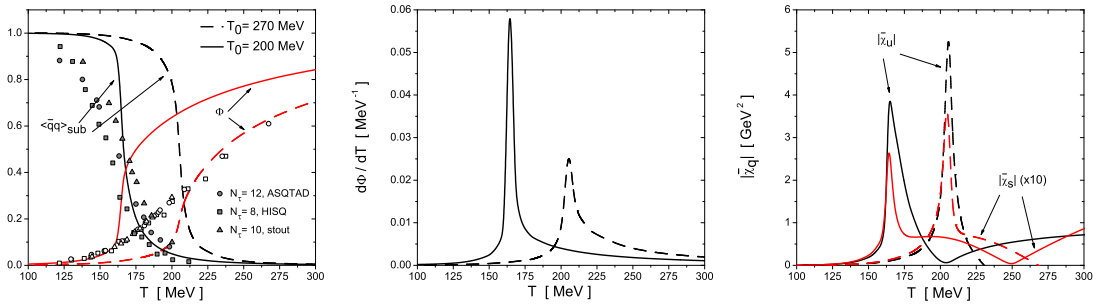

Figure 2. Subtracted chiral condensate, Polyakov loop, chiral susceptibilities and PL susceptibility $d\Phi/dT$ as functions of the temperature. Solid (dashed) curves correspond to PII, for a logarithmic PL potential with $T_0 = 200$ (270) MeV. Triangles, circles and squares stand for lattice QCD results from Refs. [19, 20].

In order to compare the features of parameterizations PI and PII, it is useful to consider some thermodynamical quantities such as the energy and the entropy densities, which can be

obtained from the thermodynamical potential:

$$\varepsilon = \Omega + Ts \ , \qquad s = -\frac{\partial \Omega}{\partial T} \ . \tag{13}$$

Our results are shown in Fig. 3, where we plot the normalized interaction energy and entropy. It can be seen that the curves for PI show a pronounced dip at about $T \sim 300$ MeV, which is not found for PII. The comparison with lattice data turn out to favor the lattice-inspired parametrization PII, as one would have expected for consistency. We have taken here the logarithmic PL potential given by Eq. (10), with $T_0 = 200$ MeV.

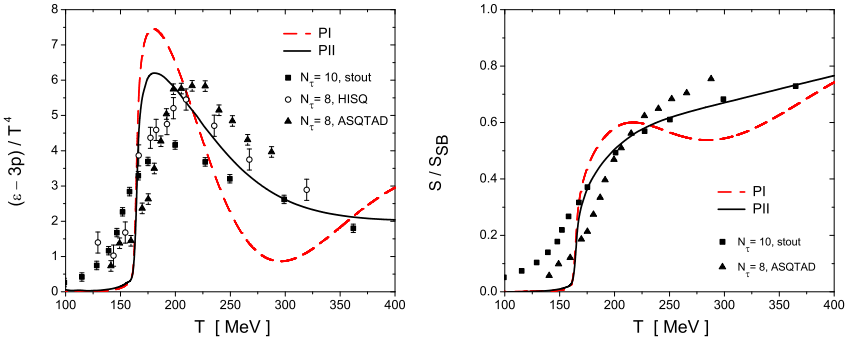

Figure 3. Normalized interaction energy (left) and entropy density (right) as functions of the temperature, for parameterizations PI and PII and a logarithmic PL potential with $T_0 = 200$ MeV. Squares, circles and triangles stand for lattice data from Refs. [20], [21] and [22], respectively.

Finally, in Fig. 4 we show the behavior of the (normalized) interaction energy, entropy density and energy density as functions of the temperature. We compare the results obtained for different PL potentials, considering the previously defined logarithmic potential as well as a widely used polynomic form (see e.g. Refs. [23, 24]) and the so-called improved polynomic potential proposed in Ref. [25]. The curves correspond to parametrization PII. It is seen that the improved polynomic potential shows a better agreement with lattice results up to the critical temperature, while for higher temperatures the agreement is better for the usual logarithmic and polynomic potentials.

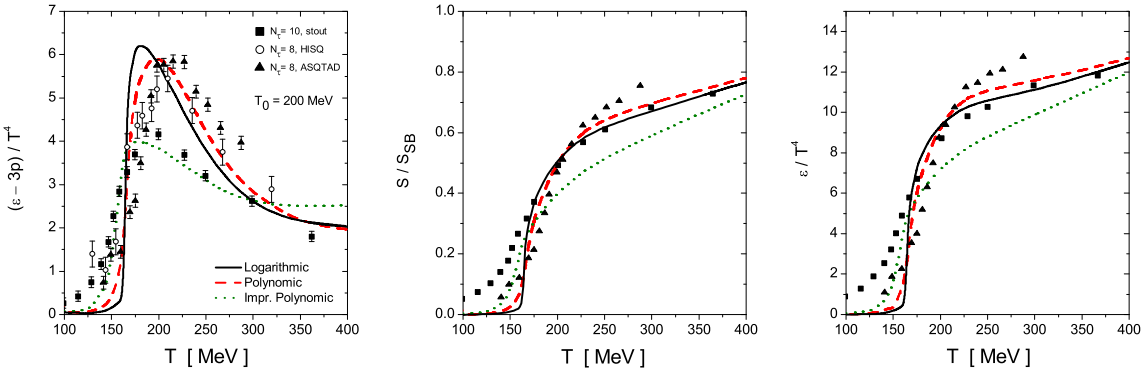

Figure 4. Normalized interaction energy, entropy density and energy density as functions of the temperature, for parameterization PII and three different PL potentials. Squares, circles and triangles stand for lattice data from Refs. [20, 21, 22].

4. Nonzero chemical potential

We have studied the phase transitions at finite chemical potential in the framework of the SU(2) version of nonlocal PNJL models. The corresponding Euclidean mean field action can be obtained from that in Eq. (1) in the limit of two flavors. Once again we consider a system at finite temperature and use the Matsubara formalism, working in the Polyakov gauge. In order to compare with lattice calculations we consider in general the case of a complex chemical potential μ. The mean field thermodynamical potential is then given by

$$\Omega^{\rm MFA}_{\rm SU(2)} = -4T \sum_{n=-\infty}^{\infty} \sum_c \int \frac{d^3\vec{p}}{(2\pi)^3} \, \log\left[\frac{(\rho^c_{n,\vec{p}})^2 + M(\rho^c_{n,\vec{p}})^2}{Z(\rho^c_{n,\vec{p}})^2}\right] + \frac{\bar{\sigma}^2 + \bar{\zeta}^2}{2\,G} + \mathcal{U}(\Phi, \Phi^*, T) \ , \quad (14)$$

where we have defined

$$\left(\rho^c_{n,\vec{p}}\right)^2 = \left[(2n+1)\pi T - i\mu + \phi_c\right]^2 + \vec{p}^{\,2} \ . \quad (15)$$

The sum over color indices runs over $c = r, g, b$, with $\phi_r = \phi_3 + \phi_8/\sqrt{3}$, $\phi_g = -\phi_3 + \phi_8/\sqrt{3}$, $\phi_b = -2 + \phi_8/\sqrt{3}$. Here ϕ_3 and ϕ_8 parametrize the traced PL according to

$$\Phi = \frac{1}{3}\left[\exp\left(-\frac{2i}{\sqrt{3}}\frac{\phi_8}{T}\right) + 2\,\exp\left(\frac{i}{\sqrt{3}}\frac{\phi_8}{T}\right)\cos(\phi_3/T)\right]. \quad (16)$$

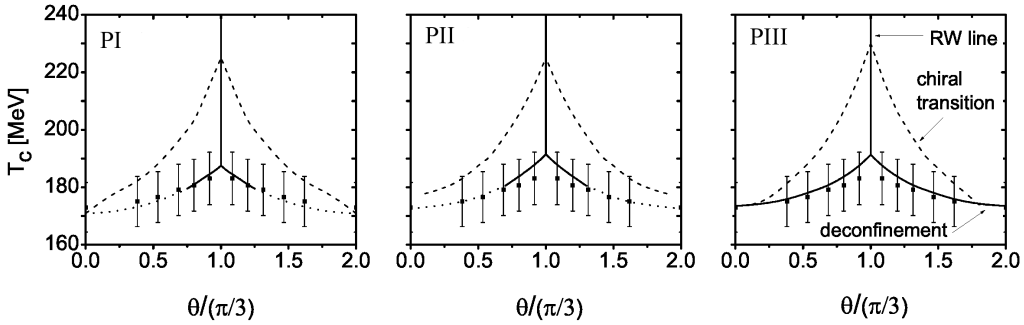

Figure 5. Critical temperature as a function of $\theta/(\pi/3)$ for parametrizations PI (left), PII (center) and PIII (right). Solid and dashed lines stand for first order and crossover-like transitions, respectively, while dots correspond to lattice QCD results [28]. Vertical solid lines correspond to the first order RW transition.

Let us first consider a purely imaginary chemical potential parametrized as $\mu = i\theta T$. In this case the QCD thermodynamical potential is invariant under the so-called extended Z_3 symmetry [26], which is a combination of a Z_3 transformation of the quark and gauge fields and a shift $\theta \to \theta + 2k\pi/3$, with integer k. It turns out that this symmetry is also present in our nlPNJL model. In QCD with dynamical quarks, if the temperature is larger than a certain value T_{RW} it can be seen that three Z_3 vacua appear. Roberge and Weiss showed that there is a first order phase transition at $\theta = \pi/3$ mod $2\pi/3$, in which the vacuum jumps to one of its Z_3 images. This is known as the "Roberge-Weiss transition", and the point at the end of the RW transition line in the (T, θ) plane, i.e. $(T, \theta) = (T_{RW}, \pi/3)$, is known as the "RW endpoint". The order of the RW transition at the RW endpoint has been subject of considerable interest recently in the framework of lattice QCD [27] due to the implications it might have

on the QCD phase diagram at finite real μ. According to lattice calculations, it appears that for two light flavors the RW endpoint is first order for realistically small values of the current quark mass. In Fig. 5 we show the dependence of the chiral restoration and deconfinement transition temperatures with θ, together with lattice data. We consider gaussian and lattice inspired parameterizations PI and PII, and also a gaussian parametrization PIII with no WFR, whereas for the PL potential we take the logarithmic form with $T_0 = 200$ MeV. We observe that, while for PIII both transitions are always first order, in the case of PI and PII there is a value $\theta_{\rm CEP} \sim 0.7 \times \pi/3$ below which the transitions become crossover-like. Thus, we find that for all three parametrizations the RW endpoint is a triple point, being the RW transition first order there. If we choose $T_0 = 270$ MeV instead, we observe qualitatively the same behavior, however the critical temperature turns out to be too high compared to lattice QCD results. Regarding the effect of different PL potentials, the main difference we find is that for the polynomic potential there are no first order deconfinement transitions, which implies a second order RW transition at the RW endpoint, in contradiction with lattice QCD predictions.

We turn now to consider the case of finite real chemical potential. In order to account for both the case of real and imaginary μ in a single plot, in Fig. 6 we show the results for the phase transition curves in the $T - \mu^2$ plane. The curves correspond to PII and a logarithmic PL potential with $T_0 = 200$ MeV. Finally, in Fig. 7 we include various $T - \mu$ phase diagrams for real μ in order to present a more detailed comparison between the results obtained for different form factors (parametrizations PI, PII and PIII in upper, center and lower panel, respectively) and PL potentials (polynomic and logarithmic, in the left and right panels respectively). Full lines correspond to first order phase transitions, dashed lines to pure chiral restoration crossover transitions, dotted lines to pure deconfinement crossover transitions, and dash-dotted lines to simultaneous chiral restoration and deconfinement crossover transitions. By increasing the chemical potential, it is seen that for both PI and PII the chiral restoration and deconfinement transitions occur at approximately the same temperature, until they reach a critical end point. The position of this point depends on the parametrization, ranging from $\mu = 150$ to 250 MeV, and from $T = 120$ to 170 MeV for $T_0 = 200$ MeV. In the case of the model with no WFR, the assumption of a logarithmic PL potential with $T_0 = 200$ MeV leads to a first order chiral phase transition at $\mu = 0$ in contradiction with lattice QCD results.

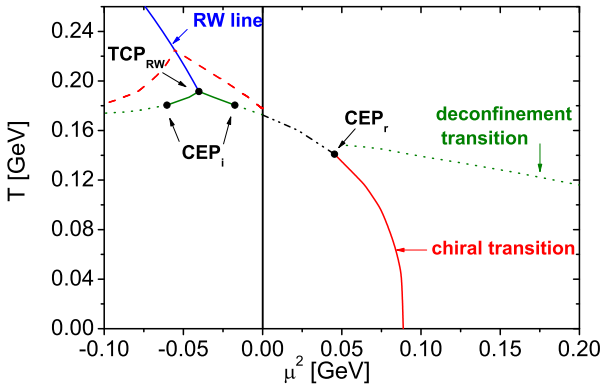

Figure 6. Phase diagram in $T - \mu^2$ space. Full lines correspond to first order phase transitions, dashed lines to pure chiral restoration crossover transitions, dotted lines to pure deconfinement crossover transitions, and dash-dotted lines to simultaneous chiral restoration and deconfinement crossover transitions. Curves correspond to PII and logarithmic PL potential with $T_0 = 200$ MeV.

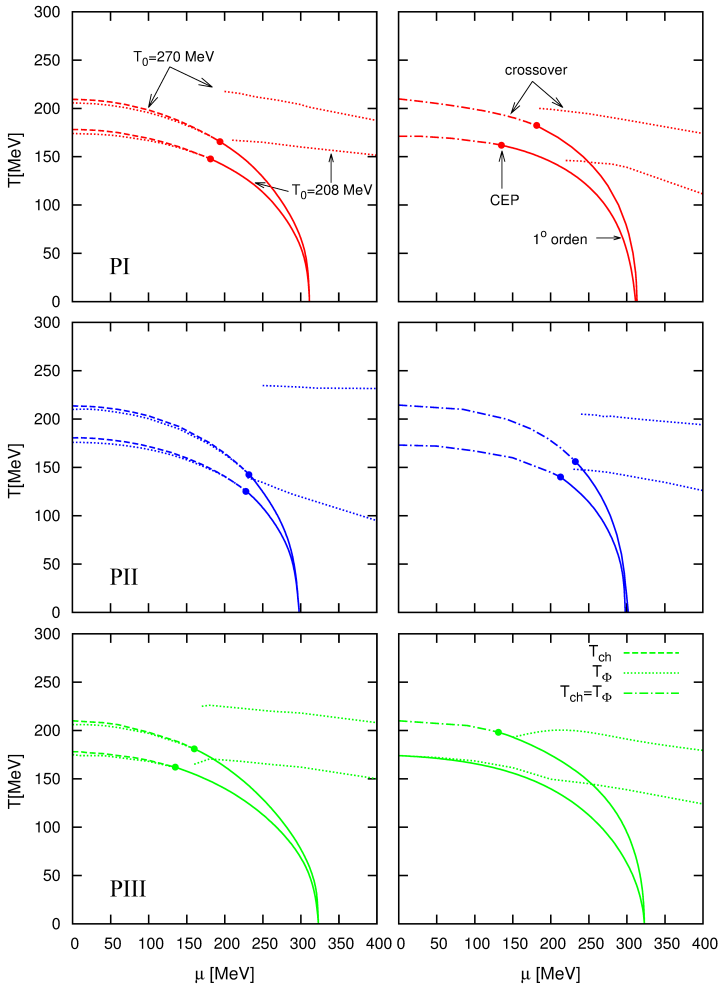

Figure 7. Phase diagrams for the three parameterizations considered. PI and PIII correspond to exponential form factors while PII to lattice motivated form factors. Full (dotted) lines correspond to first (second) order chiral restoration transitions, while dashed lines correspond to deconfinement transitions.

5. Summary

We have analyzed the features of three-flavor nlPNJL models that include wave function renormalization in the effective quark propagators. In this framework, we have obtained a parametrization (PII) of the model that reproduces lattice QCD results for the momentum dependence of the effective quark mass and WFR, and at the same time leads to an acceptable phenomenological pattern for particle masses and several meson properties in both the scalar and pseudoscalar meson sectors.

As a second step we have analyzed the characteristics of the deconfinement and chiral restoration transitions at finite temperature. In general it has been found that both transitions occur at the same critical temperature, in agreement with lattice QCD results. A critical temperature of about 170 MeV, consistent with that arising from lattice QCD calculations, has been obtained for $T_0 \simeq 200$ MeV, in agreement with theoretical expectations for a model with two/three light dynamical quarks. It is seen that the lattice-inspired power-like parameterization

PII shows indeed the best agreement with lattice QCD results.

Finally, we have considered the case of nonzero chemical potential. For imaginary chemical potentials we have analyzed the Roberge Weiss transition, which has been found to be first order at the RW endpoint for the considered parametrizations. In the case of real chemical potentials we have shown the features of the corresponding phase diagrams. At low μ, for PI and PII it is seen that chiral restoration and deconfinement transitions proceed approximately at the same critical temperatures, up to a critical end point whose location is rather dependent on the model parametrization.

Acknowledgments

This work has been partially funded by CONICET (Argentina) under grants PIP 00682 and PIP 00449, and by ANPCyT (Argentina) under grant PICT11-03-00113.

References

[1] Allton C R *et al.* 2003 *Phys. Rev.* D **68** 014507; *Phys. Rev.* D **71** 054508.
[2] Fodor Z and Katz S D 2004 *JHEP* **0404** 050; Aoki Y, Fodor Z, Katz S D and Szabo K K 2006 *JHEP* **0601** 089
[3] Karsch F and Laermann E, in *Quark Gluon Plasma III*, edited by R.C. Hwa and X. N. Wang (World Scientific, Singapore, 2004), arXiv:hep-lat/0305025
[4] Blaschke D, Buballa M, Radzhabov A E and Volkov M K 2008 *Yad. Fiz.* **71** 2012 [*Phys. Atom. Nucl.* **71** 1981]
[5] Contrera G A, Gomez Dumm D and Scoccola N N 2008 *Phys. Lett.* B **661** 113
[6] Contrera G A, Gomez Dumm D and Scoccola N N 2010 *Phys. Rev.* D **81** 054005
[7] Hell T, Roessner S, Cristoforetti M and Weise W 2009 *Phys. Rev.* D **79** 014022
[8] Hell T, Rossner S, Cristoforetti M and Weise W 2010 *Phys. Rev.* D **81** 074034
[9] Contrera G A, Orsaria M and Scoccola N N 2010 *Phys. Rev.* D **82** 054026
[10] Pagura V, Gomez Dumm D and Scoccola N N 2012 *Phys. Lett.* B **707** 76
[11] Pagura V, Gomez Dumm D and Scoccola N N 2013 *Phys. Rev.* D **87** 014027
[12] Scarpettini A, Gomez Dumm D and Scoccola N N 2004 *Phys. Rev.* D **69** 114018
[13] Hell T, Kashiwa K and Weise W 2011 *Phys. Rev.* D **83** 114008
[14] Carlomagno J P, Gomez Dumm D and Scoccola N N 2013 *Phys. Rev.* D **88** 074034
[15] Noguera S and Scoccola N N 2008 *Phys. Rev.* D **78** 114002
[16] Parappilly M B, Bowman P O, Heller U M, Leinweber D B, Williams A G and Zhang J B 2006 *Phys. Rev.* D **73** 054504
[17] Roessner S, Ratti C and Weise W 2007 *Phys. Rev.* D **75** 034007
[18] Schaefer B -J, Pawlowski J M and Wambach J 2007 *Phys. Rev.* D **76** 074023, Schaefer B -J, Wagner M and Wambach J 2010 *Phys. Rev.* D **81** 074013
[19] Borsanyi S *et al.* [Wuppertal-Budapest Collaboration] 2010 *JHEP* **1009** 073
[20] Bazavov A *et al.* [HotQCD Collaboration] 2010 *J. Phys. Conf. Ser.* **230** 012014
[21] Bazavov A *et al.* 2009 *Phys. Rev.* D **80** 014504
[22] Borsanyi S, Endrodi G, Fodor Z, Jakovac A, Katz S D, Krieg S, Ratti C and Szabo K K 2010 *JHEP* **1011** 077
[23] Scavenius O, Dumitru A and Lenaghan J T 2002 *Phys. Rev.* C **66** 034903
[24] Ratti D, Thaler M A and Weise W 2006 *Phys. Rev.* D **73** 014019
[25] Haas L M, Stiele R, Braun J, Pawlowski J M and Schaffner-Bielich J 2013 *Phys. Rev.* D **87** 076004
[26] Roberge A, Weiss N 1986 *Nucl. Phys.* B **275** 734
[27] D'Elia M, Di Renzo F, Lombardo M P 2007 *Phys. Rev.* D **76** 114509
D'Elia M, Sanfilippo F 2009 *Phys. Rev.* D **80** 111501; de Forcrand P, Philipsen O 2010 *Phys. Rev. Lett.* **105** 152001; Bonati C, Cossu G, D'Elia M and Sanfilippo F 2011 *Phys. Rev.* D **83** 054505
[28] Wu L -K, Luo X -Q, Chen H -S 2007 *Phys. Rev.* D **76** 034505